3-D honeycomb NiCo2S4 with high electrochemical performance used for supercapacitor electrodes

3-D honeycomb $NiCo_2S_4$ with high electrochemical performance used for supercapacitor electrodes

Zhiguo Zhang[a] ,Xiao Huang[a], Huan Li[a], Yingyuan Zhao[b] andTingli Ma*[a]

[a] *Department of Life Science and System Engineering, Kyushu Institute of Technology, Kitakyushu 8080134, Japan. Email: tinglima@life.kyutech.ac.jp*

[b] *School of Petroleum and Chemical Engineering, Dalian University of Technology, 124221, China.*

ABSTRACT

A new nanostructured 3-D honeycomb $NiCo_2S_4$ (NC-1) has been successfully prepared by a simple hydrothermal method assisted sulfuration procedure. The morphology of the 3-D honeycomb was investigated by FESEM and TEM, and the results suggest the NC-1 has a highly porous structure. Its chemical composition was characterized by XRD and XPS and the results indicate that the NC-1 is the pure phase of $NiCo_2S_4$. In order to study the effect of morphology on the electrochemical performance, we have also prepared needle-, flake- and petal-like nanostructured $NiCo_2S_4$ on Ni foam. When they were used as supercapacitor electrodes, the NC-1 exhibited the highest electrochemical performance among these four kinds of electrodes. Its maximum specific capacity was over 14 mAh cm^{-2} at 1 mA m^{-2} and it still yielded 7.96 mAh cm^{-2} even at 50 mA cm^{-2}. The NC-1 remained 99.64% of the initial capacity after the long-term test of 1000 cycles. Consequently, the NC-1 has the promising potential as an energy storage system in the future and it can also be used as an ideal substrate for other active materials involving a faradaic process.

Keywords: 3-D honeycomb $NiCo_2S_4$; needle-like and flake-like nanostructure; stability; supercapacitor

1. Introduction

Energy is closely related to all kinds of aspects in our daily life, and consequently, energy storage is a very vital issue [1-4]. With the increased demand for effective, safe and benign store energy, supercapacitors have been attracting attention because of their long-term stability, fast charge rate,

friendly to the environment and safety[5, 6]. Supercapacitors are bridges between batteries and traditional capacitors, therefore, they could have a high power density and energy density[7, 8]. The energy in supercapacitors can be stored either by double layer capacitors (EDLCs) or pseudo-capacitors. However, EDLCs, in which the capacity is due to the reversible ion adsorption on porous carbonaceous electrodes, have a limited specific capacity, while pseudo-capacitors, storing energy by a faradaic reaction between the active material and electrolyte, could provide a much higher capacitance than the EDLCs[9]. Transitional metal oxides, for example MnO_2, having a faradaic behavior during the charge storage process, are used as electrode materials for pseudo-capacitors[10-13]. However, their intrinsic conductivity is poor, limiting the power density and reducing the cycling performance[5, 9, 10, 14]. In order to achieve a much higher capacity and rate performance, electrode materials having a high electronic conductivity are necessary.

Recently, transitional metal sulfides have been identified as alternative electrode materials for high performance supercapacitors[15-17]. It has been demonstrated that nickel sulfide and cobalt sulfide are good electrode materials for supercapacitors which possess an excellent electrochemical performance[18, 19]. It is noted that when the $NiCo_2S_4$ is used as an electrode material, the supercapacitors have a much higher conductivity and significant redox properties than using the corresponding single component sulfide as electrode materials[20, 21]. Various $NiCo_2S_4$ with different morphologies, such as a nanosheet, nanotube and nanosphere, have been reported. These $NiCo_2S_4$ show good electrochemical properties [15, 22-25]. Wang and coworkers synthesized $NiCo_2S_4$ nanotube arrays aligned on carbon fiber paper for supercapacitor electrodes, which presented an area specific capacitance of less than 1 F cm^{-2} at 4 mA cm^{-2}[26]. Li and coworkers prepared $NiCo_2S_4$ arrays on Ni foam and the specific capacitance was over 5 F cm^{-2} at 2 mA cm^{-2}[27]. Lemu Girma Beka obtained cockscomb flower-like $NiCo_2S_4$, and it manifested 4.1 F cm^{-2} at a 2.4 mA cm^{-2} current density[28]. It is known that the redox process reacts on an active material surface or near-surface, therefore the 3-D nanostructured $NiCo_2S_4$ possessing an

effective surface area will inevitably reveal a better electrochemical performance with respect to the 1D and 2D counterparts. Meanwhile, it can retain the original structure under long-time and high loading current conditions.

In this study, 3-D honeycomb $NiCo_2S_4$ materials have been designed and synthesized by a modified hydrothermal method accompanied by a sulfuration procedure. Unlike other reporters, the substrate Ni foam was fixed on a "base" in the whole process. Due to that base, the 3-D honeycomb $NiCo_2S_4$ materials can be robustly grown on a Ni substrate without any organic binder, which could ensure a strong mechanical adhesion and electrical contact with the conductive substrate. These reasonable synthesis processes could avoid inactive area and improve the utilization of the active materials even at a high loading current. When the 3-D honeycomb $NiCo_2S_4$ materials on a Ni foam substrate are directly used as supercapacitor electrodes, the supercapacitor shows an excellent electrochemical performance; the maximum specific capacity is significant greater than 14 mAh cm^{-2}, and remains at 99.64% of the initial capacity after a long-term life test.

2. Experimental

2.1 Preparation of $NiCo_2S_4$ with different morphologies

All the reagents of analytical grade were used without further purification.

Preparation of $NiCo_2S_4$ precursor on Ni foam: Ni foam was cut into two pieces with a specific configuration. The one whose size was 35*30 mm was used as the substrate and the other was selected as the base. They were then washed in acetone, 0.1M HCl, ethanol and deionized water (DI water) in sequence with the assistance of sonication for 15 min, except for the acid at 30 min. For a typical synthesis of the $NiCo_2S_4$ precursor, 4 mmol $NiCl_2 \cdot 6H_2O$ and 8 mmol $CoCl_2 \cdot 6H_2O$ were magnetically stirred in 160 mL of DI water, followed by adding a calculated amount of NH_4F and 48 mm urea. The mixed solution was then transferred to a Teflon-lined stainless steel autoclave (TLSSA) loaded with pre-treated Ni foams and maintained at 100℃ for 5 h. After cooling to ambient temperature, the sample was

washed 3 times while sonicated. It should be noticed that the Ni substrate should be tightly fixed on its base even under the condition of high temperature and high pressure. Therefore, the $NiCo_2S_4$ can be uniformly grown on the substrate.

Preparation of $NiCo_2S_4$ on Ni foam: the precursor on the Ni foam was directly transferred into 60 mL DI water with 0.3902 g Na_2S, then sealed and maintained in the TLSSA at 160℃ for 12 h. Finally, the sample was washed and dried in a vacuum oven.

A series of experiments were performed under the same condition other than the amount of NH_4F and the samples were indexed, which was discussed in the results section.

2.2 Characterization

The crystal structure and chemical and physical compositions of the as-prepared $NiCo_2S_4$ were characterized by powder X-ray diffraction (XRD; RIGAKU), and the chemical state and elemental composition were studied by X-ray photoelectron spectroscopy (XPS; KRATOS). The morphology was observed by a field emission scanning electron microscope (FESEM; HITACHI). The transmission electron microscopy (TEM) images were recorded by a JEM-F200 (JEOL) operated at 200 kV. The electrochemical performance was conducted in a three-electrode system using a Solartron 1287/1255B.

2.3 Electrochemical measurements

The electrochemical property of all the electrodes was studied in 3 M KOH using a three-electrode system with an Hg/HgO and a piece of platinum gauze(2*2 cm^2) as the reference electrode and counter electrode, respectively. $NiCo_2S_4$ on the Ni foam was cut into 1*1 cm^2 pieces and directly employed as the working electrode. Each sample prior to testing was treated under vacuum for 30 min. Cyclic voltammograms (CV) and galvanostatic charge-discharge (GCD) curves were obtained using a Solartron 1287 and 1255B electrochemical station, and the GCD curves, which were carried out at different current densities in a fixed potential window, were used to calculate the specific capacities. Electrochemical

impedance spectroscopy (EIS) was recorded by a Solartron 1255B. The specific capacities of electrodes could be obtained from their discharge curves according to Eq. (1) as follows:

$$C=\triangle t\times I$$

where I (mA cm^{-2}) refers to the current density; $\triangle$ t (s) is the discharge time.

3. Results and discussion

The Fig. 1 simply illustrates the typical fabrication procedure of the $NiCo_2S_4$. In this process, the initial Ni foam with a smooth surface was first covered by the pink Ni-Co carbonate hydroxide precursor through the reaction of cations (Ni^{2+} and Co^{2+}) and anions (CO_3^{2-} and OH^-) when they were subjected to a hydrothermal reaction at 100℃[15, 29]. Remarkably, the metal carbonate hydroxide is in situ grown on Ni foam surface which contacted with the base instead of the other side (a curved section without pink materials in the Fig. S1). The precursors can then be hydrothermally converted to the black $NiCo_2S_4$ by the anion-exchange reaction [15]. Finally, a series of $NiCo_2S_4$ materials on Ni foam with different morphologies were fabricated. Their morphologies were characterized by FESEM and TEM, as shown in the Fig. 2, 3 and Fig. 4.

The low magnification (Fig. 2a and 2b) shows that the original smooth Ni foam is uniformly covered by a highly well-defined honeycomb structure on a large scale. From the high resolution FESEM (Fig. 2c and 2d) images, we can observe that the NC-1 is indeed composed of countless interconnected honeycomb holes and the diameter of the honeycomb is about 100-200 nm. The Fig.3 presented TEM images. The Fig. 3a and 3b illustrate NC-1 has network-like structure and it is much more obviously in the Fig. 3c. The highly well-developed 3-D honeycomb structure not only provides much more electroactive sites for the faradaic process, but also effectively shortens the distance of the charge transfer and ion diffusion to the active material surface [30]. Furthermore, NC-1 grew in situ on the conductive

Ni substrate surface, therefore, the 3-D materials can accommodate relatively high stress and volume change. When employed as an integrated electrode, it could show a high specific capacity and long stability.

As a comparison, needle-like, flake-like and petal-like $NiCo_2S_4$ materials, indexed as NC-2, NC-3 and NC-4 on Ni foam have also been prepared, as shown in the Fig. 4. Based on a low magnification, the Ni substrates are evenly coated with arrays of NC-2, NC-3 and NC-4. It can be seen that NC-2, NC-3 and NC-4 do not have a criss-crossed porous structure, which is different from the NC-1. Consequently, the NC-2, 3 and NC-4 has less active sites located at the surface or near the surface for the electrochemical reaction. The TEM images of the NC-2 and NC-3 are listed in the supporting materials. The electrochemical performances of these four $NiCo_2S_4$ materials will be discussed later.

It is apparent that NH_4F plays a vital role to synthesize these sorts of morphologies in our experiment. Just as depicted in the Fig. 5, a conclusion about the growth mechanism can be made as follows; when the amount of NH_4F was very limited, the surface of Ni foam can be activated into effective sites for crystal nucleus growth, and the nucleus just grew up along 1-D direction. As the amount of NH_4F was increased, the partial needle surface was also activated into the active sites, the nucleus grew up along 2-D direction and finally became into flakes (Fig. S4). When the amount of NH_4F was sequentially increased, the flake became shorter (Fig. 4i). While the amount of NH_4F reached to a certain level, all the needle surface was activated into the active sites, the nucleus grew up along 3-D direction. The redundant F^- would etch and shuttle through the bulk materials and finally NC-1 was obtained. Equally important consideration is that the Ni substrate and the base should be tightly fixed in TLSSA (Fig. S1). Therefore the substrate can keep still even under harsh conditions, which is very important to prepare $NiCo_2S_4$ with uniform morphologies.

The XRD patterns of NC-1, NC-2, NC-3 and NC-4 are shown in the Fig. 6. The strong diffraction peaks can be readily indexed to the (311), (400), (511) and (440) planes of the cubic $NiCo_2S_4$ phase [30].

In addition, the other of 3 remarkable peaks around 44.5°, 52.0° and 76.6° should belong to the Ni foam. The XRD patterns demonstrate that $NiCo_2S_4$ was successfully synthesized. XPS was further performed to evaluate the chemical composition of the NC-1. Details are shown in the Fig. S8.The full range pattern in the Fig. S8a indicates that NC-1 is composed of Ni, Co and S elements. The C peak is due to the carbon tape[31]. The Ni 2p high-resolution spectra could be fitted with two spin-orbit doublets of Ni^{2+} and Ni^{3+} and two corresponding shake-up satellites. The binding energy difference of Ni $2p_{3/2}$ and Ni $2p_{1/2}$ is 20.0 eV, indicating the co-existence of di/tri-valent state. Likewise, in the Co 2p spectra, the strong peaks demonstrate Co^{2+} and Co^{3+} co-existing in the NC-1. According to the S 2p analysis, the strong peaks can be attributed to S^{2-} [25, 29, 32].The XPS results are consistent with the XRD pattern.

The general electrochemical performances of the Ni foam and the four products were characterized by CV and GCD and the results in the Fig.7a show the CV curves of Ni foam and NC-1, NC-2, NC-3, NC-4 at 50 mV s^{-1}. It is obvious that the contribution of the Ni substrate is negligible while the NC-1 has a maximum enclosed area. The results imply that the NC-1 has the highest capacity [26, 33, 34], which can also be proved by the GCD results. As shown in the Fig. 7b, the NC-1 possesses the longest discharge time, about 4000 s. The good capacitor performance of the NC-1 can be ascribed to its unique structure, as we discussed in the Fig. 2 and Fig. 4. According to the above consideration, a comprehensive electrochemical measurement was implemented for the NC-1.

The electrochemical performances of NC-1 were characterized by CV and GCD in detail. As depicted in the Fig. 8a, the CV curves of the NC-1 at different scan rates are shown. It is noted that the shapes of the CV curves have no obvious changes with the increased scan rates. The curves at all the scan rates remarkably possess a pair of redox peaks, indicating its faradaic behaviors [28, 35, 36]. This can be explained as follows. When the working electrode undergoes a linear sweep voltage, on the one hand, its chemical reaction rate will unavoidably be accelerated, associated with an enhanced

corresponding current. On the other hand, the reactant concentration on/near electrode surface decreases. As it drops to zero, the concentration gradient reaches a maximum. Meanwhile, both the mass transfer rate and passing current achieve their maximum values. The diffusion layer then becomes thicker and the concentration gradient decreases with the increase in time. Therefore, the corresponding current gradually decreases, consequently, a peak emerges in the positive scan. In addition, we can observe that the redox peaks of the NC-1 move to more negative and positive positions when the scanning rates are improved [36-38]. This is caused by the internal resistance and concentration polarization resistance which are more evident at the higher scanning rates. The charge-discharge patterns of the NC-1 at different current densities are shown in the Fig. 8b. Every charging curve consists of two segments almost perpendicular to the X axis and a segment parallel to the X axis. The first abrupt potential change is created by the ohmic resistance due to its follow property. When a certain current passes through a working electrode, the double layer of the NC-1 is charged because of the electrochemical reaction hysteresis. The concentration polarization then gradually emerges and finally establishes. Then, there is a plateau in the charging curve. As the interface reactant is totally exhausted, the double layer is sharply recharged. Therefore, a new sudden potential appears. These results are consistent with its CV curves, suggesting that its electrochemical properties are from the faradaic reaction instead of the double layer. It can also be seen that all the curves have symmetric shapes, suggesting that the NC-1 had a high coulombic efficiency and reversibility [39-41]. The discharge curves are used to calculate its specific capacities according to the mentioned equation and the results are depicted in the Fig. 8c.

The Fig. 8c shows the area specific capacity of the NC-1. It can be seen that the maximum value even reaches more than 14 mAh cm^{-2} when the current density is 1 mA cm^{-2}. The area specific capacities become lower with the increased current densities. This may be induced by its internal resistance and deficient kinetic. However, its capacity still reaches ca.7.96 mAh cm^{-2} even at 50 mA cm^{-2}, suggesting its good conductivity and reversibility [18, 24, 39, 42]. The NC-1 electrode also has a good cyclic stability, as shown in the Fig. 8d. The cycle performance was tested by consecutive GCD processes at

10 mA cm^{-2} in the window range of 0-0.55 V for 1000 cycles. The gradual increase in the specific capacity is caused by the active process in the electrode. Although it has declined after 50 cycles, the specific capacity still retains 99.96% after 1000 cycles because of the outstanding conductivity and good reversibility in KOH. The inset in the Fig. 8d is the last 20 cycles, and the unchangeable curves demonstrate that the NC is very stable.

The impedance is tested by a Solartron 1255B and the result is presented in the Fig. 9a. The NC-1 exhibits a small x-intercept and negligible semicircle in the high frequency region, indicating its relative good conductivity. The former represents the ohmic internal resistance (R_L) due to its follow property and the latter is the charge transfer resistance according to the response time to frequency. The curve is almost perpendicular to the X axis in the low frequency area, which means good faradaic properties [43]. As shown in the Fig.9b, $lg|Z|$ is linear with $lg\omega$ in the low frequency, and the slope is -1/2. In the high frequency region, $lg|Z|$ is irrelevant to $lg\omega$, which is lgR_L. These results can be further proven by the Fig. 7c. The phase angle in the low-frequency area is 80 degrees which is in accordance with the Fig. 9a and it is equal to 0 degrees in the high-frequency region that is consistent with the Fig. 9b.

These results demonstrate that NC-1 has an outstanding electrochemical performance. It is known the morphology, chemical composition and the electrode preparation have a significant influence on its electrochemical properties [3, 30, 44-46]. The only difference between the NC-1 and the other three $NiCo_2S_4$ materials is the morphology. Therefore, it can be naturally concluded that the 3-D honeycomb structure of the NC-1 plays the most important role in affecting the electrochemical performance. The scientific advantages of the 3-D honeycomb morphology can be summarized as; First, the redox reaction can take place not only on the surface or near the surface region, but also in the bulk of active material shown in the Fig. 10; second, the 3-D nanostructure of the NC-1has many effective sites for the redox reaction; third, its thickness is suitable for OH^- penetration, which further increases the utilization of the active materials; fourth, the charge can be immediately transferred through its developed 3-D network;

fifth, it can alleviate strain stress and volume change during the charge and discharge processes especially under high loading current densities, which further ensure its durability. Moreover, $NiCo_2S_4$ is directly in situ grown on a conductive Ni substrate without any binder and the $NiCo_2S_4$ itself has a good conductivity comparable to metals [47].

4. Conclusion

We have successfully synthesized a series of $NiCo_2S_4$ electrode material, grown in situ on Ni foam. The obtained NC-1with a 3-D structure has the proper thickness and a developed 3-D network. When the NC-1 was used as an electrode, the specific capacity is greater than 14 mAh cm^{-2} at the current density of 1 mA cm^{-2} and the capacity retains 99.64% of the initial capacity after a long-term life test. This study provides a new nanostructured 3-D honeycomb $NiCo_2S_4$ as a promising candidate for energy storage systems. The new nanostructured 3-D honeycomb $NiCo_2S_4$ also can be used as a conductive substrate for other active materials in supercapacitors due to its unique structure and good conductivity.

Acknowledgements

This work was supported by the Grant-in-Aid for Scientific Research (KAKENHI) program, Japan (C, Grant Number 15K05597).

References

[1] A. Bello, O.O. Fashedemi, D.Y. Momodu, F. Barzegar, T.M. Masikhwa, M.J. Madito, F. Taghizadeh, J.K. Dangbegnon, N. Manyala, Electrochemical Studies of Microwave Synthesised Bimetallic Sulfides Nanostructures As Faradaic Electrodes, Electrochimica Acta, 174 (2015) 778-786.
[2] D.J. Yu, Y.F. Yuan, D. Zhang, S.M. Yin, J.X. Lin, Z. Rong, J.L. Yang, Y.B. Chen, S.Y. Guo, Nickel cobalt sulfide Nanotube Array on Nickel Foam as Anode Material for Advanced Lithium-Ion Batteries, Electrochimica Acta, 198 (2016) 280-286.
[3] E. Umeshbabu, G. Rajeshkhanna, G.R. Rao, Urchin and sheaf-like NiCo2O4 nanostructures: Synthesis and electrochemical energy storage application, International Journal of Hydrogen Energy, 39 (2014) 15627-15638.
[4] X.-P. Gao, H.-X. Yang, Multi-electron reaction materials for high energy density batteries, Energy & Environmental Science, 3 (2010) 174-189.
[5] F. Deng, J. Tie, B. Lan, M. Sun, S. Peng, S. Deng, B. Li, W. Sun, L. Yu, NiCo2O4 / MnO2 heterostructured nanosheet: influence of preparation conditions on its electrochemical properties, Electrochimica Acta, 176 (2015) 359-368.
[6] H. Wang, C. Wang, C. Qing, D. Sun, B. Wang, G. Qu, M. Sun, Y. Tang, Construction of carbon-nickel cobalt sulphide hetero-structured arrays on nickel foam for high performance asymmetric supercapacitors, Electrochimica Acta, 174 (2015) 1104-1112.
[7] V.H. Nguyen, C. Lamiel, J.-J. Shim, Hierarchical mesoporous graphene@Ni-Co-S arrays on nickel foam for high-performance supercapacitors, Electrochimica Acta, 161 (2015) 351-357.
[8] V.H. Nguyen, J.-J. Shim, In situ growth of hierarchical mesoporous NiCo2S4@MnO2 arrays on nickel foam for high-performance supercapacitors, Electrochimica Acta, 166 (2015) 302-309.
[9] V.H. Nguyen, J.-J. Shim, Three-dimensional nickel foam/graphene/NiCo2O4 as high-performance electrodes for supercapacitors, Journal of Power Sources, 273 (2015) 110-117.
[10] Y. Li, D. Cao, Y. Wang, S. Yang, D. Zhang, K. Ye, K. Cheng, J. Yin, G. Wang, Y. Xu, Hydrothermal deposition of manganese dioxide nanosheets on electrodeposited graphene covered nickel foam as a high-performance electrode for supercapacitors, Journal of Power Sources, 279 (2015) 138-145.
[11] Y. Zhu, X. Ji, Z. Wu, Y. Liu, NiCo2S4 hollow microsphere decorated by acetylene black for high-performance asymmetric supercapacitor, Electrochimica Acta, 186 (2015) 562-571.
[12] Z. Wu, X. Pu, X. Ji, Y. Zhu, M. Jing, Q. Chen, F. Jiao, High Energy Density Asymmetric Supercapacitors From Mesoporous NiCo2S4 Nanosheets, Electrochimica Acta, 174 (2015) 238-245.
[13] J. Liang, K. Xi, G. Tan, S. Chen, T. Zhao, P.R. Coxon, H.-K. Kim, S. Ding, Y. Yang, R.V. Kumar, J. Lu, Sea urchin-like NiCoO2@C nanocomposites for Li-ion batteries and supercapacitors, Nano Energy, 27 (2016) 457-465.
[14] M. Yu, J. Chen, Y. Ma, J. Zhang, J. Liu, S. Li, J. An, Hydrothermal synthesis of NiCo2O4 nanowires/nitrogen-doped graphene for high-performance supercapacitor, Applied Surface Science, 314 (2014) 1000-1006.
[15] J. Xiao, L. Wan, S. Yang, F. Xiao, S. Wang, Design Hierarchical Electrodes with Highly Conductive NiCo2S4 Nanotube Arrays Grown on Carbon Fiber Paper for High-Performance Pseudocapacitors, Nano Letters, 14 (2014) 831-838.
[16] L. Huang, D. Chen, Y. Ding, S. Feng, Z.L. Wang, M. Liu, Nickel–Cobalt Hydroxide Nanosheets Coated on NiCo2O4 Nanowires Grown on Carbon Fiber Paper for High-Performance Pseudocapacitors, Nano Letters, 13 (2013) 3135-3139.
[17] L. Zhou, H. Cao, S. Zhu, L. Hou, C. Yuan, Hierarchical micro-/mesoporous N- and O-enriched carbon derived from disposable cashmere: a competitive cost-effective material for high-performance electrochemical capacitors, Green Chemistry, 17 (2015) 2373-2382.
[18] R. Zou, Z. Zhang, M.F. Yuen, J. Hu, C.-S. Lee, W. Zhang, Dendritic Heterojunction Nanowire Arrays for High-Performance Supercapacitors, Scientific Reports, 5 (2015) 7862.
[19] Y. Gao, L. Wang, W. Zhang, X. Yang, Y. Ma, J. Shao, Y. Li, Ni-Co nanosheets supported on conductive “core” for integrated supercapacitor with high performance, Electrochimica Acta, 201 (2016) 260-267.
[20] Y. Tang, S. Chen, S. Mu, T. Chen, Y. Qiao, S. Yu, F. Gao, Synthesis of Capsule-like Porous Hollow Nanonickel Cobalt Sulfides via Cation Exchange Based on the Kirkendall Effect for High-Performance Supercapacitors, ACS Applied Materials & Interfaces, 8 (2016) 9721-9732.
[21] Y. Xiao, D. Su, X. Wang, L. Zhou, S. Wu, F. Li, S. Fang, In suit growth of ultradispersed NiCo2S4 nanoparticles on graphene for asymmetric supercapacitors, Electrochimica Acta, 176 (2015) 44-50.
[22] Q. Chu, W. Wang, X. Wang, B. Yang, X. Liu, J. Chen, Hierarchical NiCo2O4@nickel-sulfide nanoplate arrays for high-performance supercapacitors, Journal of Power Sources, 276 (2015) 19-25.
[23] R. Jin, D. Liu, C. Liu, G. Liu, Hierarchical NiCo2S4 hollow spheres as a high performance anode for lithium ion batteries, RSC Advances, 5 (2015) 84711-84717.
[24] R. Zou, Z. Zhang, M.F. Yuen, M. Sun, J. Hu, C.-S. Lee, W. Zhang, Three-dimensional-networked NiCo2S4 nanosheet array/carbon cloth anodes for high-performance lithium-ion batteries, NPG Asia Mater, 7 (2015) e195.
[25] Z. Zeng, D. Wang, J. Zhu, F. Xiao, Y. Li, X. Zhu, NiCo2S4 nanoparticles//activated balsam pear pulp for asymmetric hybrid capacitors, CrystEngComm, 18 (2016) 2363-2374.
[26] Y. Huang, T. Shi, S. Jiang, S. Cheng, X. Tao, Y. Zhong, G. Liao, Z. Tang, Enhanced cycling stability of NiCo2S4@NiO core-shell nanowire arrays for all-solid-state asymmetric supercapacitors, Scientific Reports, 6 (2016) 38620.
[27] R. Li, S. Wang, Z. Huang, F. Lu, T. He, NiCo2S4@Co(OH)2 core-shell nanotube arrays in situ grown on Ni foam for high performances asymmetric supercapacitors, Journal of Power Sources, 312 (2016) 156-164.
[28] L.G. Beka, X. Li, W. Liu, In situ grown cockscomb flower-like nanostructure of NiCo2S4 as high performance supercapacitors, Journal of Materials Science: Materials in Electronics, 27 (2016) 10894-10904.
[29] Z. Yang, X. Zhu, K. Wang, G. Ma, H. Cheng, F. Xu, Preparation of NiCo2S4 flaky arrays on Ni foam as binder-free supercapacitor electrode, Applied Surface Science, 347 (2015) 690-695.
[30] H. Chen, J. Jiang, L. Zhang, D. Xia, Y. Zhao, D. Guo, T. Qi, H. Wan, In situ growth of NiCo2S4 nanotube arrays on Ni foam for supercapacitors: Maximizing utilization efficiency at high mass loading to achieve ultrahigh areal pseudocapacitance, Journal of Power Sources, 254 (2014) 249-257.
[31] X.F. Gong, J.P. Cheng, K.Y. Ma, F. Liu, L. Zhang, X. Zhang, Nanostructured nickel-cobalt sulfide grown on nickel foam directly as supercapacitor electrodes with high specific capacitance, Materials Chemistry and Physics, 173 (2016) 317-324.
[32] N. Huang, S. Zhang, H. Huang, J. Liu, Y. Sun, P. Sun, C. Bao, L. Zheng, X. Sun, X. Zhao, Pt-sputtering-like NiCo2S4 counter electrode for efficient dye-sensitized solar cells, Electrochimica Acta, 192 (2016) 521-528.
[33] T. Zhu, E.R. Koo, G.W. Ho, Shaped-controlled synthesis of porous NiCo2O4 with 1-3 dimensional hierarchical nanostructures for high-performance supercapacitors, RSC Advances, 5 (2015) 1697-1704.
[34] W. Li, L. Xin, X. Xu, Q. Liu, M. Zhang, S. Ding, M. Zhao, X. Lou, Facile synthesis of three-dimensional structured carbon fiber-NiCo2O4-Ni(OH)2 high-performance electrode for pseudocapacitors, Scientific Reports, 5 (2015) 9277.
[35] F. Lu, M. Zhou, W. Li, Q. Weng, C. Li, Y. Xue, X. Jiang, X. Zeng, Y. Bando, D. Golberg, Engineering sulfur vacancies and impurities in NiCo2S4 nanostructures toward optimal supercapacitive performance, Nano Energy, 26 (2016) 313-323.
[36] L. Niu, Y. Wang, F. Ruan, C. Shen, S. Shan, M. Xu, Z. Sun, C. Li, X. Liu, Y. Gong, In situ growth of NiCo2S4@Ni3V2O8 on Ni foam as a binder-free

electrode for asymmetric supercapacitors, Journal of Materials Chemistry A, 4 (2016) 5669-5677.
[37] D. Cai, D. Wang, C. Wang, B. Liu, L. Wang, Y. Liu, Q. Li, T. Wang, Construction of desirable NiCo2S4 nanotube arrays on nickel foam substrate for pseudocapacitors with enhanced performance, Electrochimica Acta, 151 (2015) 35-41.
[38] L. Li, Nanoscience, Materials Technology, 30 (2015) A51-A52.
[39] T. Wang, Y. Guo, B. Zhao, S. Yu, H.-P. Yang, D. Lu, X.-Z. Fu, R. Sun, C.-P. Wong, NiCo2O4 nanosheets in-situ grown on three dimensional porous Ni film current collectors as integrated electrodes for high-performance supercapacitors, Journal of Power Sources, 286 (2015) 371-379.
[40] X. Liu, S. Shi, Q. Xiong, L. Li, Y. Zhang, H. Tang, C. Gu, X. Wang, J. Tu, Hierarchical NiCo2O4@NiCo2O4 Core/Shell Nanoflake Arrays as High-Performance Supercapacitor Materials, ACS Applied Materials & Interfaces, 5 (2013) 8790-8795.
[41] X. Lu, X. Huang, S. Xie, T. Zhai, C. Wang, P. Zhang, M. Yu, W. Li, C. Liang, Y. Tong, Controllable synthesis of porous nickel-cobalt oxide nanosheets for supercapacitors, Journal of Materials Chemistry, 22 (2012) 13357-13364.
[42] R. Zou, M.F. Yuen, L. Yu, J. Hu, C.-S. Lee, W. Zhang, Electrochemical Energy Storage Application and Degradation Analysis of Carbon-Coated Hierarchical NiCo2S4 Core-Shell Nanowire Arrays Grown Directly on Graphene/Nickel Foam, Scientific Reports, 6 (2016) 20264.
[43] Q. Wang, X. Wang, J. Xu, X. Ouyang, X. Hou, D. Chen, R. Wang, G. Shen, Flexible coaxial-type fiber supercapacitor based on NiCo2O4 nanosheets electrodes, Nano Energy, 8 (2014) 44-51.
[44] B. Yang, L. Yu, H. Yan, Y. Sun, Q. Liu, J. Liu, D. Song, S. Hu, Y. Yuan, L. Liu, J. Wang, Fabrication of urchin-like NiCo2(CO3)1.5(OH)3@NiCo2S4 on Ni foam by an ion-exchange route and application to asymmetrical supercapacitors, Journal of Materials Chemistry A, 3 (2015) 13308-13316.
[45] H. Niu, D. Zhou, X. Yang, X. Li, Q. Wang, F. Qu, Towards three-dimensional hierarchical ZnO nanofiber@Ni(OH)2 nanoflake core-shell heterostructures for high-performance asymmetric supercapacitors, Journal of Materials Chemistry A, 3 (2015) 18413-18421.
[46] J. Xiao, X. Zeng, W. Chen, F. Xiao, S. Wang, High electrocatalytic activity of self-standing hollow NiCo2S4 single crystalline nanorod arrays towards sulfide redox shuttles in quantum dot-sensitized solar cells, Chemical Communications, 49 (2013) 11734-11736.
[47] C. Xia, P. Li, A.N. Gandi, U. Schwingenschlögl, H.N. Alshareef, Is NiCo2S4 Really a Semiconductor?, Chemistry of Materials, 27 (2015) 6482-6485.

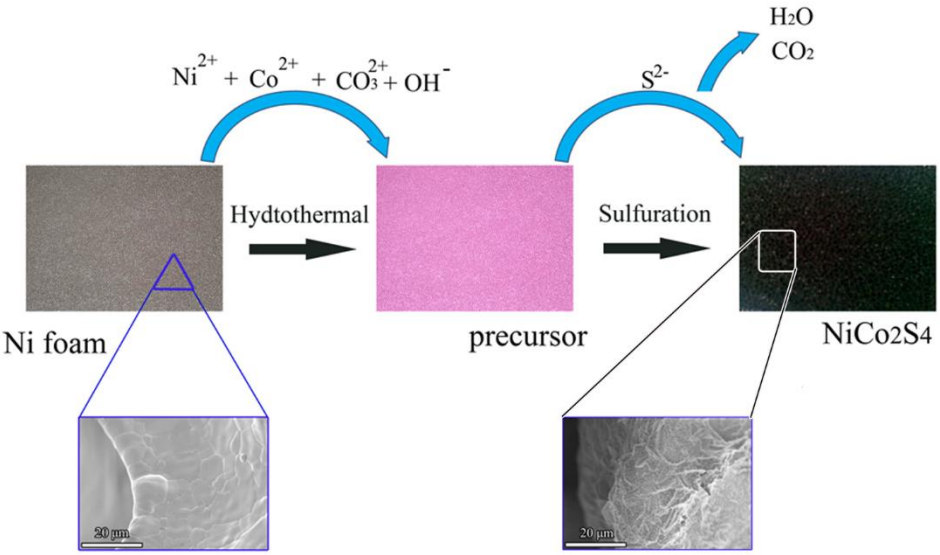

Fig.1 Schematic illustration of the synthesis route towards $NiCo_2S_4$ on Ni foam

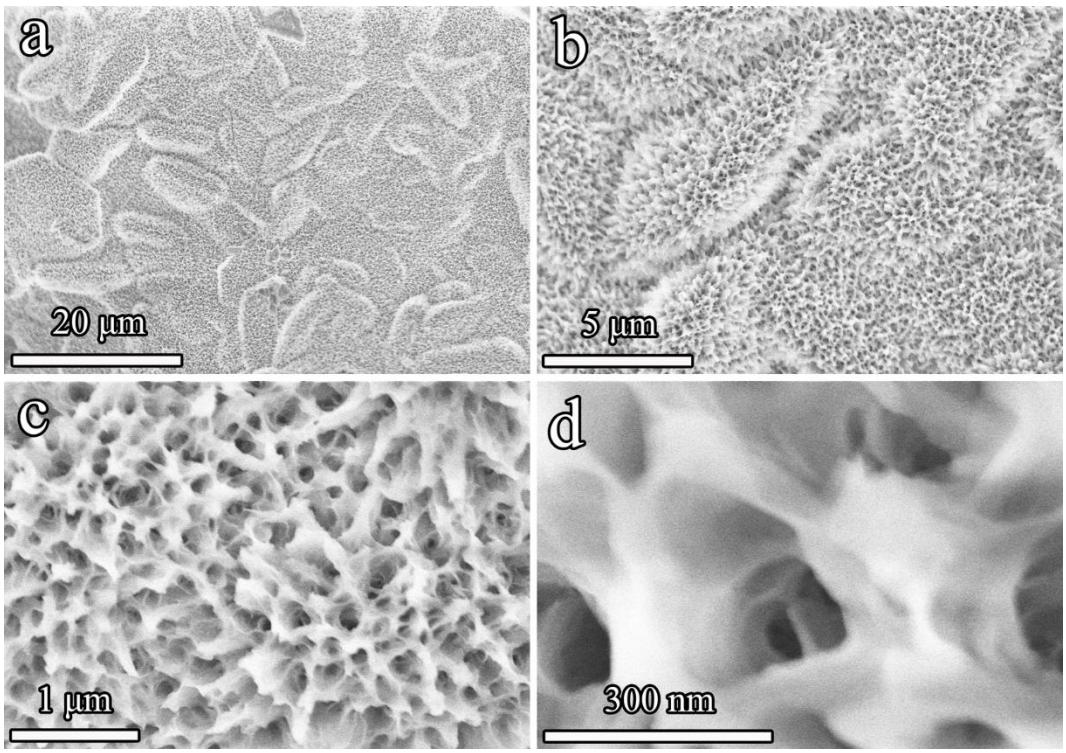

Fig. 2 FESEM of NC-1

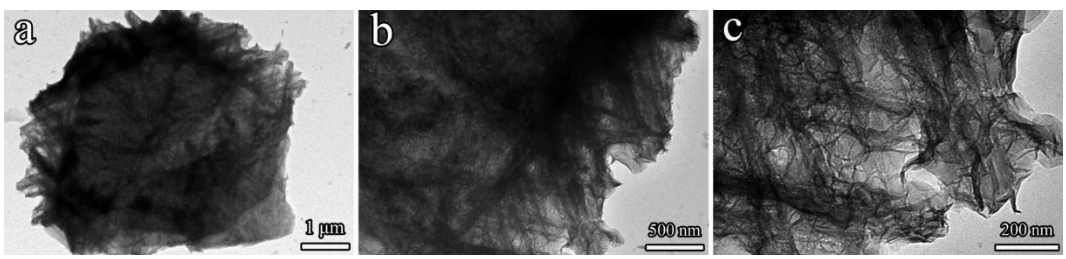

Fig.3 TEM of NC-1

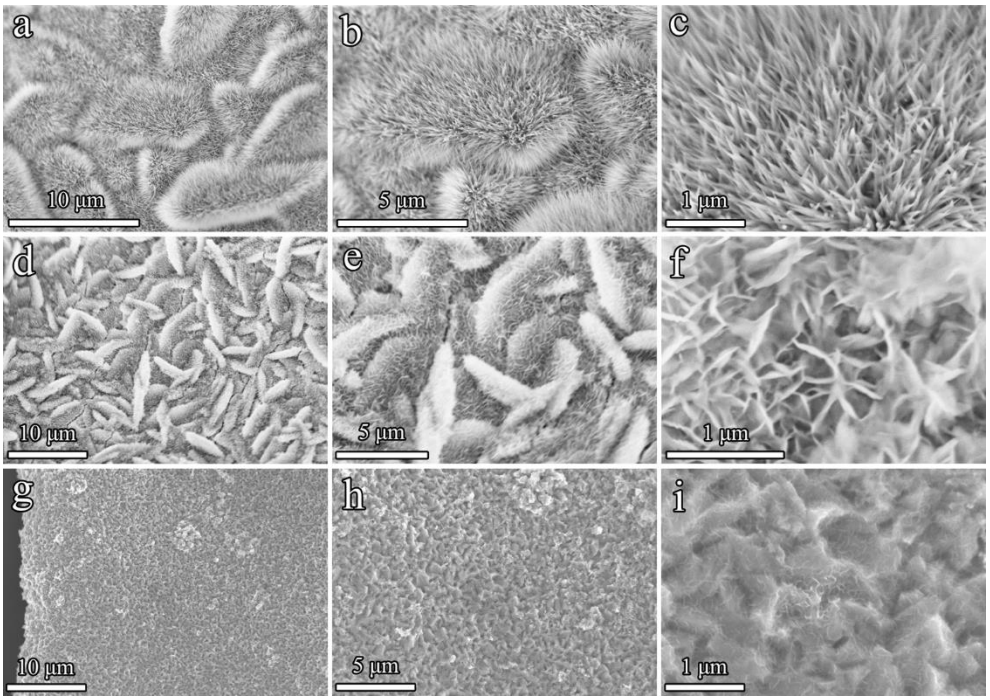

Fig.4 FESEM images of (a-c) NC-2, (d-f) NC-3 and (g-i) NC-4

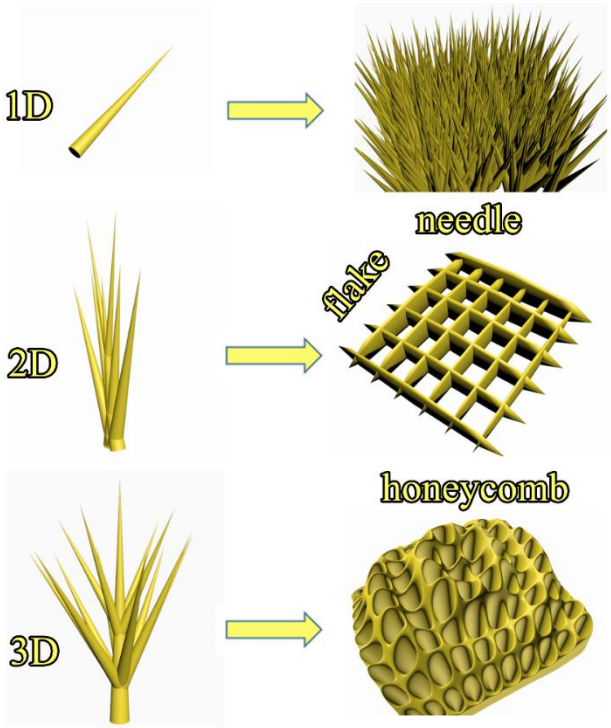

Fig.5 Possible mechanism for fabrication $NiCo_2S_4$ with different morphologies.

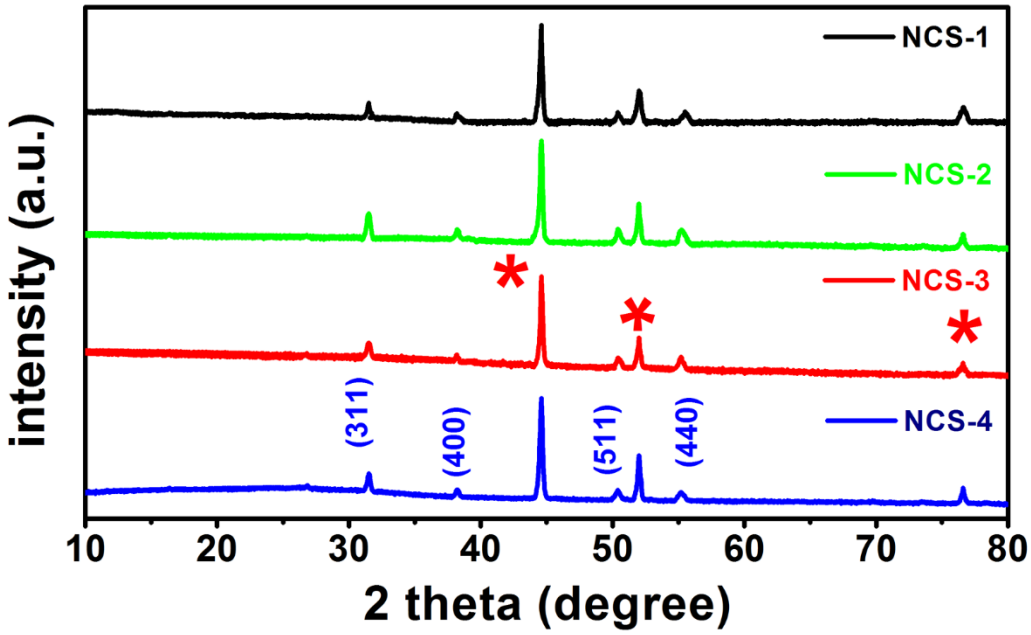

Fig.6 XRD pattern of NC-1, NC-2, NC-3 and NC-4.

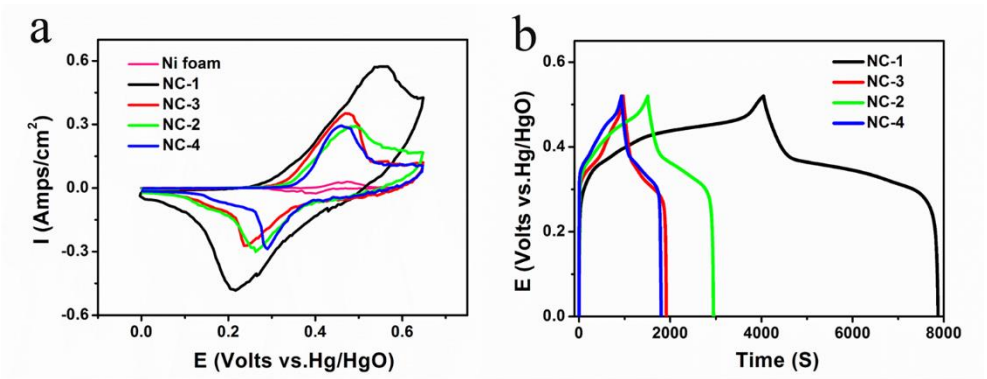

Fig.7 (a) The comparison of CV curves (after 10 cycles) from Ni foam to NC-4; (b) GCD curves of NC-1, NC-2, NC-3, NC-4 under 1 mA cm^{-2}

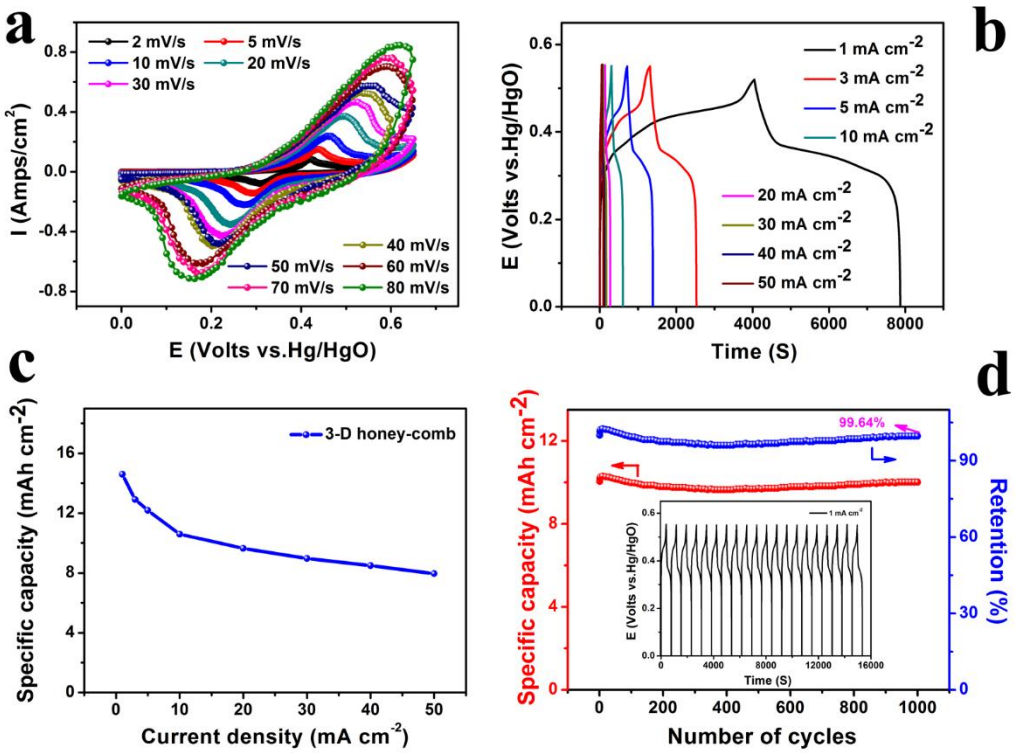

Fig.8 Electrochemical performance of NC-1: (a) cyclic voltammograms (CV) curves (after 10 cycles) at different scanning rates (2, 5, 10, 20, 30, 40, 50, 60, 70, 80 mV s^{-1}); (b) galvanostatic charge-discharge (GCD) curves (after 10 cycles) under diverse charge/discharge current densities (1, 3, 5, 10, 20, 30, 40, 50 mA cm^{-2}); (c) area capacity as a function of the current density and (d) its cycle performance at 10 mA cm^{-2}.

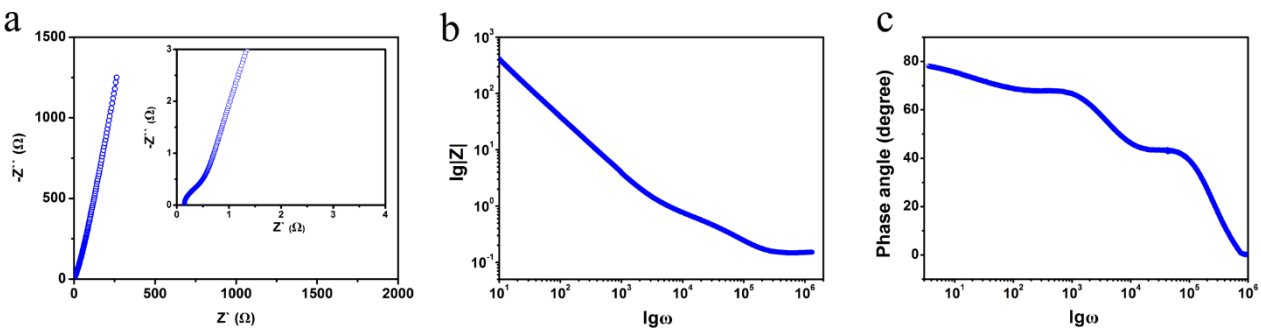

Fig.9 (a) Nyquist profile, (b and c) bode plot module and phase of impedance versus frequency for NC-1

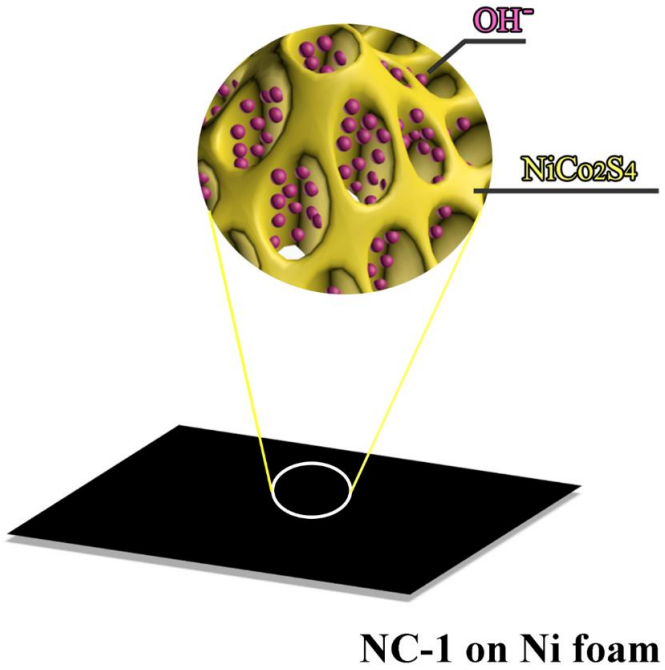

Fig.10 Illustration of the reaction of NC-1 and OH^- in the electrochemical process